The Journal of Chemical Physics

Simulation of the single-vibronic-level emission spectrum of HPS

Cite as: J. Chem. Phys. **140**, 194311 (2014); https://doi.org/10.1063/1.4875806
Submitted: 20 March 2014 . Accepted: 29 April 2014 . Published Online: 20 May 2014

Daniel K. W. Mok, Edmond P. F. Lee, Foo-tim Chau, and John M. Dyke

Simulation of the single-vibronic-level emission spectrum of HPS

Daniel K. W. Mok,[1,a)] Edmond P. F. Lee,[1,2,a)] Foo-tim Chau,[1] and John M. Dyke[2]
[1]*Department of Applied Biology and Chemical Technology, The Hong Kong Polytechnic University, Hung Hom, Hong Kong*
[2]*School of Chemistry, University of Southampton, Highfield, Southampton SO17 1BJ, United Kingdom*

(Received 20 March 2014; accepted 29 April 2014; published online 20 May 2014)

We have computed the potential energy surfaces of the $\tilde{X}^1A'$ and $\tilde{A}^1A''$ states of HPS using the explicitly correlated multi-reference configuration interaction (MRCI-F12) method, and Franck–Condon factors between the two states, which include anharmonicity and Duschinsky rotation, with the aim of testing the assignment of the recently reported single-vibronic-level (SVL) emission spectrum of HPS [R. Grimminger, D. J. Clouthier, R. Tarroni, Z. Wang, and T. J. Sears, J. Chem. Phys. **139**, 174306 (2013)]. These are the highest level calculations on these states yet reported. It is concluded that our spectral simulation supports the assignments of the molecular carrier, the electronic states involved and the vibrational structure of the experimental laser induced fluorescence, and SVL emission spectra proposed by Grimminger *et al.* [J. Chem. Phys. **139**, 174306 (2013)]. However, there remain questions unanswered regarding the relative electronic energies of the two states and the geometry of the excited state of HPS. © *2014 AIP Publishing LLC*. [http://dx.doi.org/10.1063/1.4875806]

INTRODUCTION

Very recently, Grimminger *et al.* have reported the $\tilde{A}^1A'' - \tilde{X}^1A'$ laser induced fluorescence (LIF) and single-vibronic-level (SVL) emission spectra of HPS and DPS.[1] In order to assist spectral assignments, density functional theory (DFT) calculations, and both single-reference (SR) and multi-reference (MR) *ab initio* calculations were carried out.[1] In addition, anharmonic Franck–Condon factors (FCFs) between the two states involved were computed with a "quick and dirty" approach (their quotes; see Ref. 1 for details), employing computed coupled-cluster single and double plus perturbative triples {CCSD(T)} and complete active space self-consistent field multi-reference configuration interaction (including Davidson corrections) (CASSCF/MRCI) potential energy functions (PEFs) for the two electronic states, respectively, using the augmented correlation consistent polarized valence quadruple-zeta {aug-cc-pV(Q+d)Z} basis set. However, although computed FCFs of the $\tilde{A}^1A'' \leftarrow \tilde{X}^1A'(0, 0, 0)$ excitation of HPS and DPS were published in Ref. 1, a direct comparison between the computed FCFs and experimental LIF spectra of HPS and DPS could not be made, because the observed LIF spectra were not corrected for laser power. Nevertheless, Ref. 1 has reported the 3_0^4 SVL emission spectrum of HPS, though not the corresponding computed anharmonic FCFs. In this connection, in the present study, we have carried out FCF calculations, in order to simulate the vibrational structure of the 3_0^4 SVL emission spectrum of HPS, with the aim of testing the assignments proposed in Ref. 1. We have used our *ab initio*/FCF method[2–4] successfully to provide "fingerprint" type assignments of SVL emission spectra of numerous triatomic molecules,[5–12] including HPO/DPO,[13] which are valence iso-electronic with HPS/DPS. In addition, it should be noted that, CCSD(T) and explicitly correlated CCSD(T)-F12 calculations on HPS, its cation and anion, in their ground electronic states, were also published roughly at the same time as Ref. 1, together with their CCSD(T)/aug-cc-pV5Z PEFs and anharmonic vibrational energies.[14] These recent publications[1,14] demonstrate the recent interest in HPS, specifically as a species of interest in the interstellar medium and astrochemistry,[14] and an important molecule for understanding the bonding in molecules composed of second row elements.

COMPUTATIONAL DETAILS

CASSCF/MRCI-F12 calculations

The explicitly correlated CASSCF/MRCI-F12 (including Davidson corrections)[15,16] method, as implemented in MOLPRO,[17] was employed, because the $\tilde{A}^1A''$ state of HPS is an open-shell singlet state, which requires a MR method. In addition, explicitly correlated methods are known to achieve a dramatic improvement of basis set convergence of correlation energies, when compared with conventional correlation methods (such as MRCI).[18,19] The cc-pVQZ-F12[20] (or VQZ-F12) and cc-pCVQZ-F12[21] (or CVQZ-F12) atomic orbital (AO) basis sets, specifically designed for F12 methods, were used in geometry optimization, together with the corresponding density fitting (DF: aug-cc-pVQZ-MP2FIT and aug-cc-pwCVQZ-MP2FIT)[22,23] and resolution of the identity (RI: cc-pVQZ_OPTRI and cc-pCVQZ-F12_OPTRI)[21,24] basis sets (see MOLPRO online manual[17]). With the VQZ-F12 AO basis sets, a full valence active space was employed in CASSCF and subsequent MRCI-F12 calculations. With the CVQZ-F12 AO basis sets for P and S, a full valence active space was used in CASSCF calculations, but the $2s^22p^6$ core electrons of both P and S were correlated explicitly in subsequent MRCI-F12 calculations. Also, with the VQZ-F12 basis set, the default value of 1.0 was used for the geminal Slater exponent {β, in

a)Authors to whom correspondence should be addressed. Electronic addresses: bcdaniel@polyu.edu.hk and epl@soton.ac.uk

the nonlinear correlation factor, $\hat{F}_{(r_{12})} = -(1/\beta)\exp(-\beta r_{12})\}$ in the MRCI-F12 calculation, while with the CVQZ-F12 basis set, β was set to 1.5. These choices of the F12 basis sets and corresponding β values follow recommendations from a recent investigation on basis sets and core-valence effects with explicitly correlated methods (see Ref. 21). The total numbers of contracted Gaussian functions in the CVQZ-F12 AO, DF, and RI basis sets are 258, 670, and 330, respectively. The total numbers of contracted and uncontracted configurations in the MRCI-F12 calculations performed in the present study using the CVQZ-F12 basis set are more than 28.3 million and 5.4 billion configurations, respectively.

PEFs, FCF calculations, and spectrum simulations

We computed 409 and 380 CASSCF/MRCI-F12/CVQZ-F12 energies for the $\tilde{X}^1A'$ and $\tilde{A}^1A''$ states of HPS, in the ranges of $\{1.0 \leq r(PH) \leq 2.43$ Å, $50 \leq \theta(HPS) \leq 160^\circ$, $1.4 \leq r(PS) \leq 2.9$ Å$\}$ and $\{1.1 \leq r(PH) \leq 2.5$ Å, $40 \leq \theta(HPS) \leq 145^\circ$, $1.7 \leq r(PS) \leq 2.75$ Å$\}$, respectively. They were fitted to PEFs of a polynomial form (see Refs. 8 and 13 for details; the polynomial and computed PEFs are given in Table S1 in the supplementary material[25]). Employing these PEFs and the rovibronic Hamiltonian of Watson[26] for a nonlinear molecule, anharmonic vibrational wavefunctions (expressed as linear combinations of harmonic oscillator functions) and their corresponding energies were computed. Various harmonic oscillator basis sets have been used to ensure that basis size effects on computed anharmonic vibrational energies and FCFs of interest are negligibly small. Some lower-lying computed anharmonic wavefunctions of the $\tilde{X}^1A'$ and $\tilde{A}^1A''$ states of HPS are given in the supplementary material.[25] Franck–Condon factors including anharmonicity and Duschinsky rotations were then calculated as described previously.[8,9] Vibrational components in the $\tilde{A}^1A'' - \tilde{X}^1A'$ absorption and SVL emission spectra of HPS/DPS were simulated employing computed anharmonic FCFs and frequency factors of 1 and 4, respectively, with Gaussian line shapes and a full-width-at-half-maximum of 10 cm^{-1}.[8,9]

RESULTS AND DISCUSSION

Computed geometrical parameters, relative electronic energies, and vibrational frequencies

Computed geometrical parameters and relative electronic energies are summarized in Table I. As can be seen in

TABLE I. Computed and experimentally derived geometrical parameters (r_e values, except otherwise stated) of, and excitation energies (T_e values, except otherwise stated) between, the $\tilde{X}^1A'$ and $\tilde{A}^1A''$ states of HPS.

$\tilde{X}^1A'$	HP (Å)	PS (Å)	HPS (deg)	T_e (cm^{-1})
UCCSD(T)-F12b/VQZ-F12[a]	1.4339	1.9332	101.84	
MRCI-F12/VQZ-F12[a]	1.4321	1.9361	101.98	
MRCI-F12/CVQZ-F12[a]	1.4210	1.9264	102.16	
MRCI-F12/CVQZ-F12 PEF[a]	1.4225	1.9256	102.13	
MRCI/AV(5+d)Z[1]	1.4315	1.9371	102.09	
CCSD(T)/AV(Q+d)Z PEF[1]	1.4334	1.9373	101.77	
CCSD(T)/AV(6+d)Z[14]	1.4335	1.9333	101.8	
CCSD(T)/AV5Z PEF[14]	1.4335	1.9347	102.1	
UCCSD(T)-F12b/VQZ-F12[14]	1.4335	1.9331	101.8	
CCSD(T)/cc-pwCVQZ[27]	1.4303	1.9293	101.84	
MW r_0[27]	1.444(5)	1.931(1)	101.6(5)	
MW (semi-experimental r_e)[27]	1.4321(2)	1.9287(1)	101.78(1)	
$\tilde{A}^1A''$				
MRCI-F12/VQZ-F12[a]	1.4263	2.0568	91.89	12 296
(as above) $\Delta r_e/\theta_e$[b]	− 0.0058	+0.1207	− 10.09	
MRCI-F12/CVQZ-F12[a]	1.4129	2.0512	92.34	12 939
(as above) $\Delta r_e/\theta_e$[b] and T_0[c]	− 0.0081	+0.1238	− 9.82	12 739
(as above) T_0[c] DPS				12 770
MRCI-F12/CVQZ-F12 PEF[a]	1.4227	2.0475	91.98	12 578
(as above) $\Delta r_e/\theta_e$[b] and T_0[c]	0.0003	+0.1219	− 10.14	12 378
(as above) T_0[c] DPS				12 409
MRCI/AV(Q+d)Z PEF[1]	1.4290	2.0635	91.74	
{CCSD(T) & MRCI PEF's}[1] $\Delta r_e/\theta_e$[b]	− 0.0004	+0.1262	− 10.03	
MRCI/AV(5+d)Z[1]	1.4290	2.0595	92.01	12 060
(as above)[14] T_0[c]				11 880
IFCA geometry[d]	1.424	2.155	91.5	
IFCA[d] $\Delta r_e/\theta_e$[b]	− 0.0081	+0.2263	− 10.28	
LIF T_0 (estimated)[1]				11 291

[a]Present work; see text.
[b]Geometry changes upon excitation.
[c]$T_0 = T_e + \Delta(ZPE)$, with computed ν's for $\Delta(ZPE)$.
[d]The r_e geometry of the $\tilde{X}^1A'$ state was fixed to the semi-experimental geometry,[27] while the IFCA procedure was employed to obtain the r_e geometry of the $\tilde{A}^1A''$ state (see text).

TABLE II. Computed and experimental vibrational frequencies (ω_e [ν] values in cm^{-1}) of the $\tilde{X}^1A'$ and $\tilde{A}^1A''$ states of HPS and DPS.

	HPS			DPS		
$\tilde{X}^1A'$	HP	Bend	PS	DP	Bend	PS
MRCI-F12/CVQZ-F12 PEF[a]	2298	931	695	1652	676	695
(as above) ν	[2190]	[911]	[688]	[1594]	[666]	[688]
CCSD(T)/AV(Q+d)Z PEF[1]	2274	903	684	1634	656	684
(as above; variationally) ν	[2171]	[887]	[678]	[1582]	[647]	[678.0]
MRCI/AV(5+d)Z[1]	2254	911	682			
RCCSD(T)/AV5Z PEF[14]	2273	909	686			
(as above) ν	[2263.9][b]	[894.1]	[655.9]			
CCSD(T)-F12/VQZ-F12[14]	2276	906	689			
SVL emission[1] (ω_i^0 values[c])	2178(2)[d]	900.5(10)	683.3(7)			
SVL emission[1] ν	[2177.6]	[894.5]	[682.3][e]	...	[651.7]	[682.4]
$\tilde{A}^1A''$						
MRCI-F12/CVQZ-F12 PEF[a]	2320	707	515	1666	511	515
(as above) ν	[2195]	[683]	[511]	[1601]	[499]	[511]
MRCI/AV(Q+d)Z PEF[1]	2287	694	505	1642	497	510
(as above; variationally) ν	[2168]	[674]	[500]	[1582]	[490]	[501]
LIF[1] (ω_i^0 values[c])	...	679(2)	517.3(10)			
LIF[1] ν	...	[675][f]	[515.3]			[508][g]

[a]Present study.
[b]This is most likely a mistake, as x_{11} given in Ref. 14 has a value of -64.94 cm^{-1}.
[c]The ω_i^0 values were derived using equation 2 in Ref. 1.
[d]Note that no x_{11} value is available, as only the 1_1 component was observed.
[e]Analysis of hot bands in the LIF spectrum gave an energy of 678.1(9) cm^{-1} for the 3_1 level.
[f]The 2_0^1 LIF band is weak; see Ref. 1.
[g]Separation between the 3_0^1 and 3_0^2 components.

Table I, we have also optimized the geometry of the $\tilde{X}^1A'$ state of HPS at the explicitly correlated unrestricted-spin coupled-cluster single and double plus perturbative triples (UCCSD(T)-F12) level. It is pleasing that the optimized geometrical parameters obtained at the UCCSD(T)-F12 and the MRCI-F12 levels with the VQZ-F12 basis set agree very well (differences of $\leq$0.003 Å and $\leq$0.2°). In fact, generally, all computed geometrical parameters shown in Table I, obtained with default frozen cores for P and S agree very well for both states of HPS. When core electrons of P and S are correlated explicitly, computed r_e(PH) and r_e(PS) values decrease, while computed θ_e(HPS) values increase, for both states of HPS, when compared with the corresponding values obtained with frozen cores. A similar trend is also observed from previous CCSD(T) calculations (e.g., with the AV(Q+d)Z[1] and cc-pwCVQZ[27] basis sets; Table I) for the $\tilde{X}^1A'$ state. Summing up, all computed geometrical parameters are very consistent, particularly for the computed θ_e values for both states, which have overall spreads of $\leq$0.6°. The experimental r_0 and semi-experimental r_e geometrical parameters of the $\tilde{X}^1A'$ state of HPS have been derived in a microwave study.[27] Comparing the semi-experimental r_e values with corresponding computed values (Table I), the agreement in θ_e is very good (within 0.4°). Regarding r_e(PS), the semi-experimental value agrees very well (within 0.0023 Å) with our MRCI-F12/CVQZ-F12 value. However, for r_e(PH), the semi-experimental value agrees better with the MRCI-F12/VQZ-F12 value (almost identical) than with the MRCI-F12/CVQZ-F12 value (within 0.011 Å). Also, it agrees very well with the CCSD(T)/cc-pwCVQZ value[27] (within 0.002 Å).

Regarding T_e/T_0 values, only computed values obtained at the highest levels of theory are shown in Table I (for lower level values, see Ref. 1). It should be noted that the experimental T_0 value in Ref. 1 was not obtained by direct measurement. It was derived from vibrational analysis, as the 0_0^0 band was not observed in the LIF spectrum of HPS.[1] Comparing computed and experimental T_0 values, computed values are generally larger than the experimental value, and improvements in the levels of calculation (e.g., including core correlation and/or using an explicitly correlated method, which improves basis size convergence) lead to larger discrepancies between theory and experiment. A similar observation was noted in Ref. 1. At the currently highest level, MRCI-F12/CVQZ-F12, the computed T_0 value of 12 739 cm^{-1} is 1448 cm^{-1} ($\sim$0.19 eV) larger than the derived experimental value of 11 291 cm^{-1} from Ref. 1.

Computed harmonic (ω) and fundamental (ν) vibrational frequencies of all three vibrational modes in the two states of HPS/DPS (ν_1 and ν_3 are the HP and PS stretching modes, while ν_2 is the bending mode) obtained by different methods are given in Table II. It can be seen that computed ω values have spreads as large as 44 cm^{-1} {e.g., with ω(HP) of the $\tilde{X}^1A'$ state of HPS}. Regarding computed ν values, the restricted-spin coupled-cluster single and double plus perturbative triples (RCCSD(T))/AV5Z PEF ν(HP) value of 2263.9 cm^{-1} of the $\tilde{X}^1A'$ state of HPS from Ref. 14 is most likely a mistake (see footnote b of Table II). At the same time, the derived ω_i^0(PH) value of the $\tilde{X}^1A'$ state of HPS from Ref. 1 is probably not reliable (see footnote d of Table II). Nevertheless, the agreement between

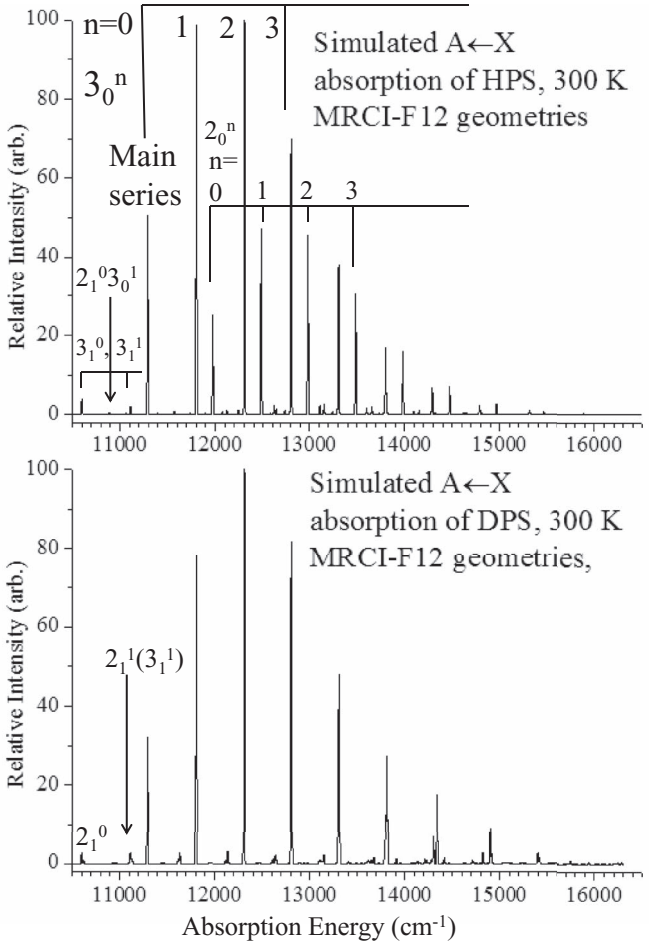

FIG. 1. Simulated absorption spectra of HPS (top) and DPS (bottom) from the $\tilde{X}^1A'$ state to the $\tilde{A}^1A''$ state employing MRCI-F12/cc-pCVQZ PEFs and geometries at 300 K.

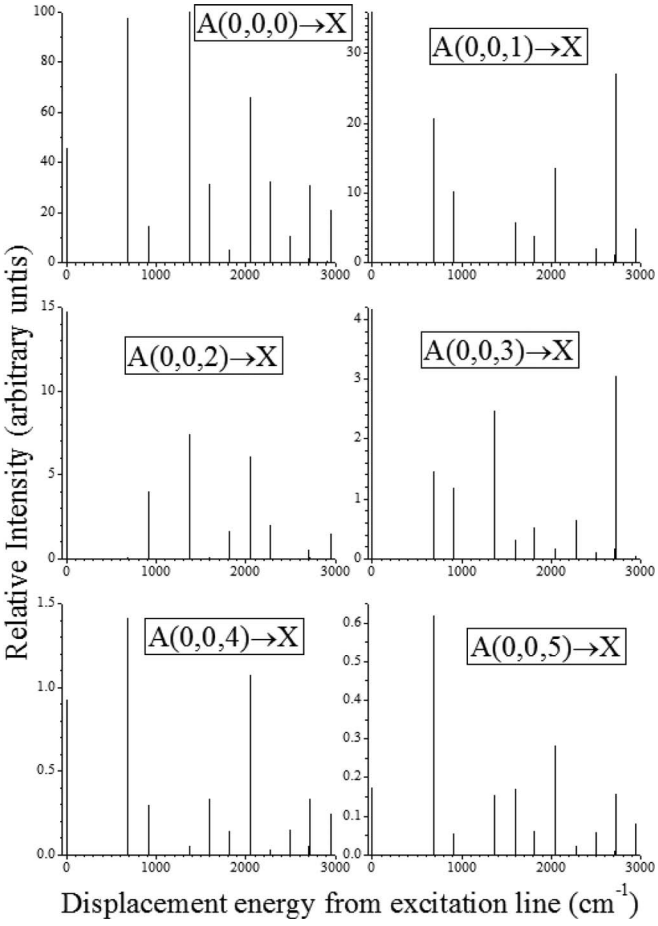

FIG. 2. Computed relative intensities (in arbitrary units; bar diagrams) of the 3_0^n (n = 0, 1, 2, 3, 4, or 5) SVL emission spectra of HPS obtained using MRCI-F12/CVQZ geometries.

computed MRCI-F12/CVQZ-F12 and available observed ν values of both states of HPS/DPS is reasonably good (within 17 cm^{-1}).

Simulated spectra

The simulated $\tilde{A}^1A'' \leftarrow \tilde{X}^1A'$ absorption spectra of HPS and DPS employing the computed MRCI-F12/CVQZ-F12 geometries for the two states involved are given in Figure 1. The simulated vibrational structures obtained here are essentially identical to the bar diagrams of the computed FCF values reported in Ref. 1 (Figure 5 therein), supporting the reliability of the "brute force" ("quick and dirty") numerical integration method used in Ref. 1. The good agreement also indicates the similar quality of the two sets of PEFs used here and in Ref. 1.

Computed relative intensities of vibrational components (bar diagrams) of the 3_0^n (n = 0, 1, 2, 3, 4, or 5) SVL emission spectra of HPS obtained using the computed MRCI-F12/CVQZ geometries are shown in Figure 2. Comparing these computed vibrational structures with the experimental 3_0^4 SVL emission spectrum of Ref. 1 (Figure 3 top trace), it is clear that the experimental spectrum cannot be due to the 3_0^0, 3_0^1, 3_0^2, or 3_0^3 SVL emission. Possibly, the experimental spectrum may be considered to match best with the simulated 3_0^4 or 3_0^5 SVL emissions. However, if the experimental SVL emission spectrum is assigned to arise from the 3_0^5 excitation, the revised extrapolated experimental T_0 value will be smaller than that reported in Ref. 1, which has assigned the experimental spectrum to arise from the 3_0^4 excitation, by one quantum in ν_3''. Consequently, the revised extrapolated T_0 value will be even further away from the computed MRCI-F12 values than the value proposed in Ref. 1. In view of this consideration, the experimental SVL emission spectrum is assigned to be from the 3_0^4 excitation, rather than the 3_0^5 excitation. In any case, the general agreement between the simulated 3_0^4 SVL $\{\tilde{A}^1A''(0, 0, 4) \rightarrow \tilde{X}^1A'\}$ emission spectra of HPS, obtained employing the MRCI-F12/CVQZ-F12 geometries, and the experimental spectrum from Ref. 1 as shown in Figure 3 (middle and top traces, respectively) is good. The only minor discrepancy lies in the relative intensity of the relatively weak $\tilde{A}^1A''(0, 0, 4) \rightarrow \tilde{X}^1A'(0, 0, 2)$ vibrational component (3_2 in Figure 3).

In order to improve the agreement between the simulated and experimental 3_0^4 SVL emission spectra, the iterative Franck–Condon analysis (IFCA) procedure[8,13] was carried out. In the IFCA procedure, the semi-experimental r_e geometry of the $\tilde{X}^1A'$ state of HPS[27] was used, while the geometrical parameters of the $\tilde{A}^1A''$ state were varied from the MRCI-F12/CVQZ-F12 geometry until a best match between the

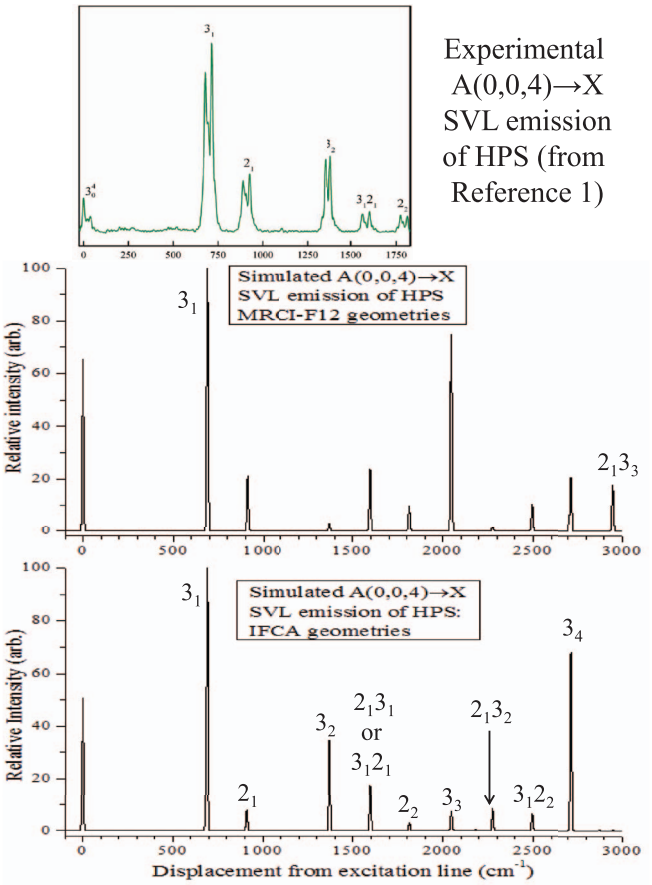

FIG. 3. Simulated 3_0^4 SVL emission spectra of HPS employing MRCI-F12/CVQZ-F12 (middle trace) and IFCA geometries (bottom trace; see text) for the $\tilde{X}^1A'$ and $\tilde{A}^1A''$ states of HPS, together with the corresponding experimental spectrum (top trace) from Ref. 1.

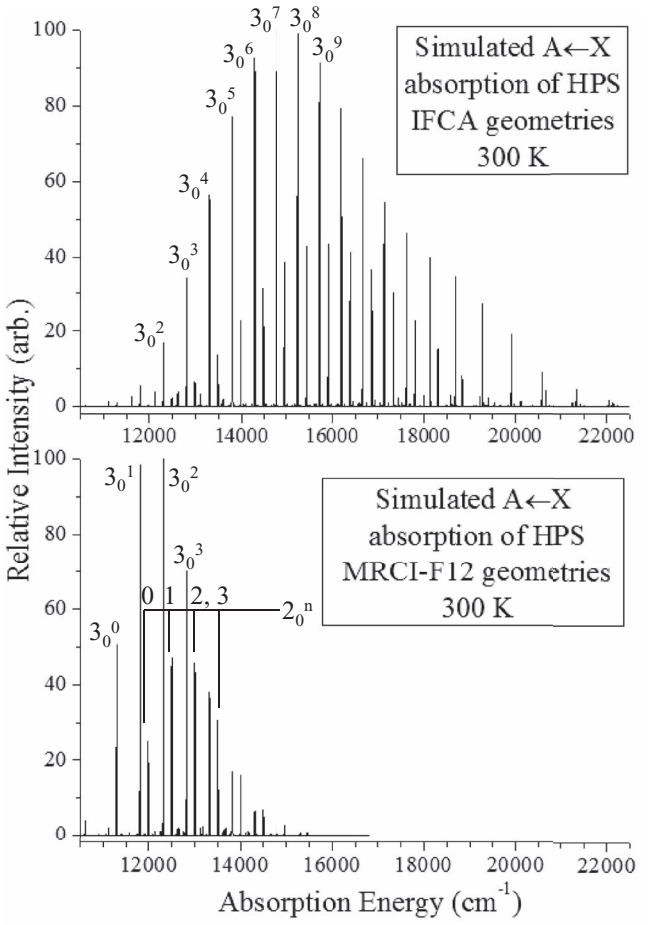

FIG. 4. Simulated absorption spectra of HPS employing MRCI-F12/CVQZ-F12 (bottom trace, as top trace of Figure 1) and IFCA geometries (top trace; see text) at 300 K.

simulated and experimental spectra was obtained (vibronic components and relative intensities). Since the published experimental spectrum covers only up to the 1800 cm^{-1} region (displacement energy from the excitation line; Figure 3 top trace), comparison between simulated and experimental spectra can only be made within this region (up to the 2_2 component). In order to increase the relative intensity of the simulated 3_2 component, the PS bond length has to be increased significantly. {Different geometry changes upon excitation ($\Delta r_e/\theta_e$) obtained by different methods are given in Table I.} Comparing the two simulated spectra obtained using two different sets of geometries (Figure 3, middle and bottom traces), the simulated vibrational structures in the low displacement energy region (<1800 cm^{-1}) are actually quite similar. They differ more at higher displacement energy, specifically in the relative intensities of the 3_3 and 3_4 components. Unfortunately, the experimental spectrum[1] (top trace of Figure 3) does not cover this energy region, because of experimental limitations (see Ref. 1 for details).

We have also simulated the absorption spectrum of HPS employing the IFCA geometries of the two states. This simulated band (Figure 4 top trace) extends to very large absorption energies {22 000 cm^{-1}, cf., ~15 000 cm^{-1} with the simulated spectrum using the MRCI-F12 geometries (Figure 2 bottom trace)}, with the band maximum at the 3_0^7 component (cf., the 3_0^2 component with the MRCI-F12 geometries). The 0_0^0 component is very weak and will be difficult to be observed experimentally. This appears to be in line with the fact that of the 0_0^0 component is not observed in the experimental LIF spectrum.

CONCLUDING REMARKS

We have computed explicitly correlated MRCI-F12 PEFs, which include core correlation, for the $\tilde{X}^1A'$ and $\tilde{A}^1A''$ states of HPS, and anharmonic FCFs, which include allowance for anharmonicity and Duschinsky rotation, between the two states. Employing computed FCFs, the 3_0^4 and also other 3_0^n SVL emission spectra of HPS were simulated and compared with the experimental 3_0^4 SVL emission spectra. The computed 3_0^4 SVL emission spectrum gives the best agreement with the experimental spectrum. It is, therefore, concluded that our spectral simulation supports the assignments of the molecular carrier, the electronic states involved, and the vibrational structure of the experimental SVL emission spectrum proposed in Ref. 1. In this connection, we have answered the first of the three unanswered questions raised in the Conclusions of Ref. 1 on the exact assignment of PS stretching quanta in the LIF spectra. However, the remaining

two questions on the exact position of the 0_0^0 band and the geometry of the excited state remain open. Regarding the 0_0^0 position, the rather large discrepancy of 0.19 eV between the computed MRCI-F12/CVQZ-F12 value and the derived experimental value is disappointing. Further experimental and theoretical investigations are required to determine the exact position of the 0_0^0 band of HPS and to resolve the discrepancy between theory and experiment on T_0. Regarding the geometry of the excited state, our IFCA geometry has a r_e(PS) value, which is larger than all high level computed values by ~0.1 Å (Table I). In addition, the IFCA geometries give a simulated absorption spectrum, which is very different from that obtained with the computed MRCI-F12/CVQZ-F12 geometries. It should be noted that the IFCA geometrical parameters were derived based on the published experimental 3_0^4 SVL emission spectrum, especially the relative intensity of the relatively weak 3_2 component. Clearly, there are some experimental limitations associated with the published SVL emission spectrum in Ref. 1. First, the 3_2 component is relatively weak. Second, the spectral range available in the experimental spectrum is rather narrow due to experimental limitations, as mentioned above. Third, some impurity bands and/or overlapping rotational structures, as shown in the experimental LIF spectrum of Ref. 1 (Figure 1 therein), may have affected the observed SVL emission spectrum. In view of the above considerations, the geometry of the upper state remains uncertain, and that obtained via the IFCA procedure should be viewed with caution. Summarizing, further spectroscopic and computational investigations will be required to establish the $\tilde{A}^1A'' \leftarrow \tilde{X}^1A'$ band origin and the geometry of the excited state of HPS. Moreover, the reasonably good agreement between the overall vibrational envelopes of the simulated and experimental SVL emission spectra indicates that the experimental spectrum arises from the 3_0^4 excitation of HPS.

ACKNOWLEDGMENTS

The authors are grateful to the RGC of HKSAR (Grant Nos. 501112 and 501813) for support. Computations were carried out using resources of the NSCCS, EPSRC (UK). Also, E.P.F.L. thanks NERC (UK) for support and J.M.D. acknowledges support from the Leverhulme Trust. Very helpful comments from Professor D. Clouthier and Professor T. Sears on our manuscript are gratefully acknowledged.

[1] R. Grimminger, D. J. Clouthier, R. Tarroni, Z. Wang, and T. J. Sears, J. Chem. Phys. **139**, 174306 (2013).
[2] D. K. W. Mok, E. P. F. Lee, F.-T. Chau, D. C. Wang, and J. M. Dyke, J. Chem. Phys. **113**, 5791 (2000).
[3] F.-T. Chau, D. K. W. Mok, E. P. F. Lee, and J. M. Dyke, ChemPhysChem **6**, 2037 (2005).
[4] D. W. K. Mok, E. P. F. Lee, F.-T. Chau, and J. M. Dyke, J. Chem. Theor. Comput. **5**, 565 (2009).
[5] D. K. W. Mok, E. P. F. Lee, F.-T. Chau, and J. M. Dyke, J. Comput. Chem. **22**, 1896 (2001).
[6] F.-T. Chau, J. M. Dyke, E. P. F. Lee, and D. K. W. Mok, J. Chem. Phys. **115**, 5816 (2001).
[7] E. P. F. Lee, D. K. W. Mok, J. M. Dyke, and F.-T. Chau, J. Phys. Chem. A **106**, 10130 (2002).
[8] D. K. W. Mok, E. P. F. Lee, F.-T. Chau, and J. M. Dyke, J. Chem. Phys. **120**, 1292 (2004).
[9] F.-T. Chau, D. K. W. Mok, E. P. F. Lee, and J. M. Dyke, J. Chem. Phys. **121**, 1810 (2004).
[10] J. M. Dyke, E. P. F. Lee, D. K. W. Mok, and F.-T. Chau, ChemPhysChem **6**, 2046 (2005).
[11] D. K. W. Mok, F.-T. Chau, E. P. F. Lee, and J. M. Dyke, J. Comput. Chem. **31**, 476 (2010).
[12] E. P. F. Lee, D. K. W. Mok, F.-T. Chau, and J. M. Dyke, J. Chem. Phys. **132**, 234309 (2010).
[13] E. P. F. Lee, D. K. W. Mok, F.-T. Chau, and J. M. Dyke, J. Chem. Phys. **127**, 214305 (2007).
[14] S. B. Yaghlane, C. E. Cotton, J. S. Francisco, R. Linguerri, and M. Hochlaf, J. Chem. Phys. **139**, 174313 (2013).
[15] T. Shiozaki and H.-J. Werner, Mol. Phys. **111**, 607 (2013).
[16] T. Shiozaki and H.-J. Werner, J. Chem. Phys. **134**, 184104 (2011).
[17] H.-J. Werner, P. J. Knowles, R. Lindh, F. R. Manby, M. Schütz *et al.*, MOLPRO, version 2012.1, a package of *ab initio* programs, 2012, see http://www.molpro.net.
[18] G. Knizia, T. B. Adler, and H.-J. Werner, J. Chem. Phys. **130**, 054104 (2009).
[19] T. Helgaker, W. Klopper, and D. P. Tew, Mol. Phys. **106**, 2107 (2008).
[20] K. A. Peterson, T. Adler, and H.-J. Werner, J. Chem. Phys. **128**, 084102 (2008).
[21] J. G. Hill, S. Mazumder, and K. A. Peterson, J. Chem. Phys. **132**, 054108 (2010).
[22] K. Weigend and C. Hättig, J. Chem. Phys. **116**, 3175 (2002).
[23] C. Hättig, Phys. Chem. Chem. Phys. **7**, 59 (2005).
[24] K. E. Yousaf and K. A. Peterson, J. Chem. Phys. **129**, 184108 (2008).
[25] See supplementary material at http://dx.doi.org/10.1063/1.4875806 for Table S1 and some computed anharmonic vibrational wavefunctions.
[26] J. K. G. Watson, Mol. Phys. **19**, 465 (1970).
[27] D. T. Halfen, D. J. Clouthier, L. M. Ziurys, V. Lattanzi, M. C. McCarthy, P. Thaddeus, and S. Thorwith, J. Chem. Phys. **134**, 134302 (2011).